Proton conductivity and stability of Ba2In2O5 in hydrogen containing atmospheres

Jankovic, Jasna; Wilkinson, David P.; Hui, Rob

Publisher's version / Version de l'éditeur:
https://doi.org/10.1149/1.3511787
Journal of The Electrochemical Society, 158, 1, pp. B61-B68, 2010-11-19

Journal of The Electrochemical Society, **158** (1) B61-B68 (2011)
0013-4651/2010/158(1)/B61/8/$28.00 © The Electrochemical Society

Proton Conductivity and Stability of $Ba_2In_2O_5$ in Hydrogen Containing Atmospheres

Jasna Jankovic,[a,b,*] David P. Wilkinson,[a,b,,z] and Rob Hui[b]**

[a]*Department of Chemical and Biological Engineering, University of British Columbia, Vancouver, British Columbia, Canada V6T 1Z3*
[b]*Institute for Fuel Cell Innovation, National Research Council Canada, Vancouver, British Columbia, Canada V6T 1W5*

$Ba_2In_2O_5$ is one of the oxygen deficient ceramic materials widely investigated for both oxygen ion conduction and proton conduction in oxidizing atmospheres. However, its electrochemical properties have not been studied in hydrogen containing atmospheres. In this work, the electrical conductivity of $Ba_2In_2O_5$ in hydrogen containing atmospheres was investigated by ac impedance spectroscopy in the temperature range between 100 and 500°C and compared to its conductivity in air and nitrogen in order to estimate the contribution of proton conductivity to the total conductivity. A stable electrical conductivity of over 0.3 S/cm was achieved in the temperature range of 300–480°C in a 50% vol H_2/50% vol N_2 atmosphere. Electromotive force measurements (and complimentary open circuit cell voltage measurements) revealed high proton transport numbers over the temperature range. $Ba_2In_2O_5$ shows chemical stability in hydrogen containing atmospheres at temperatures up to 480°C, while decomposing at higher temperatures. Mechanical instability was noticed in humid atmospheres at 400°C and above. This previously unreported high conductivity in H_2 atmosphere creates an opportunity for use of $Ba_2In_2O_5$ as a proton conductive material for a range of intermediate temperature electrochemical devices.
 [DOI: 10.1149/1.3511787]

Manuscript submitted June 15, 2010; revised manuscript received October 18, 2010. Published November 19, 2010.

Acceptor-doped perovskite oxides, ABO_3, (e.g., $BaCeO_3$, $SrCeO_3$, $BaZrO_3$, and $SrZrO_3$) have attracted significant attention because of their electrical properties.[1-3] In these materials, the ideal perovskite $A^{2+}B^{4+}O_3^{2-}$ is doped with lower-valent M^{3+} ions, forming oxygen vacancies to compensate for the charge difference.[4] Existence of the oxygen vacancies favors oxygen ion transport and causes oxygen ion conduction in these materials. Moreover, mixed oxygen-ion and proton conduction has been found in these systems, with oxygen ion conduction predominant at high temperatures (typically above 500°C) and protonic conduction predominant at low temperatures (typically below 500°C).[5-8] Fast oxide ion conduction in this class of materials is applicable for use in oxygen sensors, solid oxide fuel cells, separation membranes, and other electrochemical devices at elevated temperatures. Proton conduction can have applications in humidity sensors, proton conducting fuel cells, gas sensors, and hydrogen pumps in the intermediate temperature range (100–500°C), with many advantages in terms of cost, material stability, water management, etc. Proton conduction in acceptor-doped perovskites has been under investigation since 1981, when Iwahara et al.[6] first discovered it, but still none of these or related materials have shown satisfactory proton conduction for practical applications in the intermediate temperature range.

Brownmillerite-structured $Ba_2In_2O_5$ belongs to the same category as the acceptor-doped perovskites and is an extreme case of acceptor doping, in which B^{4+} cations are completely replaced by In^{3+} cations.[5,9-15] To maintain charge balance, one sixth of the oxygen anions are removed and a high concentration of oxygen vacancies is formed. At low temperatures, the vacancies are ordered in parallel rows (tetrahedral oxygen vacancy layers) alternating with mainly vacancy-free octahedral perovskite layers. These vacancies are treated as interstitial sites in the brownmillerite structure. Oxygen vacancies trapped in these ordered layers do not contribute extensively to the oxygen ion conduction. At temperatures above the disorder temperature, $T_d = 925$°C, oxygen vacancies become partially or completely disordered and the structure reverts to that of a highly defective cubic perovskite. Oxygen ions move through the structure much easier, greatly contributing to the enhanced ion conduction. The defect chemistry of the brownmillerite structure in $Ba_2In_2O_5$ favors both oxygen ion conduction as well as proton incorporation.[5] Its electrochemical behavior and electrical conduction have been found to be very dependent on temperature and the atmosphere. Oxygen ion, electronic, and protonic conduction have been confirmed for $Ba_2In_2O_5$ under different conditions.[5,8,16-18]

While oxygen ion conductivity of this material under different conditions is well investigated, proton conductivity has been studied only in humid air or inert gases, but not in hydrogen containing atmospheres. Zhang and Smyth[5] showed that if the conductivity is measured in moist air, $Ba_2In_2O_5$ exhibits evidence of proton conduction. Although low ($< 1 \times 10^{-5}$ S/cm), proton conductivity was found to be predominant at temperatures below 500°C. In addition, Schober et al.[11] have confirmed proton solubility in $Ba_2In_2O_5$ in moist air atmospheres at temperatures below 800°C. Although not experimentally confirmed, proton conductivity of $Ba_2In_2O_5$ in humid atmospheres has been attributed to the incorporation of water molecules from the atmosphere into the oxygen-deficient oxide structure through the following reaction, where oxygen vacancies are filled by hydroxyl ions[13]

$$H_2O_{(g)} + V_O^{\cdot\cdot} + O_O^x \Leftrightarrow 2OH_O^{\cdot} \quad [1]$$

where using Kröger–Vink notation,[19] $V_O^{\cdot\cdot}$ is an oxygen vacancy, O_O^x is the oxide ion, and $OH_O^{\cdot}$ is the hydroxyl ion. If oxygen is also present, it competes with water molecules for the available oxide ion vacancies, producing electron holes ($h^{\cdot}$) and p-type electronic conductivity, according to the reaction[4,10,16]

$$1/2O_{2(g)} + V_O^{\cdot\cdot} \Leftrightarrow O_O^x + 2h^{\cdot} \quad [2]$$

If $Ba_2In_2O_5$ is to be used as a proton conductive electrolyte in electrochemical devices such as fuel cells, it is crucial to determine its electrochemical behavior in hydrogen containing atmospheres. Although some related materials have been investigated in hydrogen atmospheres,[2,18-27] and mainly at temperatures above 500°C, this has not been done for $Ba_2In_2O_5$. The mechanism of proton creation in this and related materials in hydrogen containing atmospheres is not fully understood. Hui et al.[18] have proposed a possible mechanism for direct hydrogen incorporation in the structure via interaction with oxygen ions, forming protons (or hydroxyl ions) and electrons

$$1/2H_{2(g)} + O_O^x \Leftrightarrow OH_O^{\cdot} + e' \quad [3]$$

They suggested that hydrogen incorporated by this mechanism plays a more important role in proton conduction than that of the moisture.

* Electrochemical Society Student Member.
** Electrochemical Society Active Member.
z E-mail: dwilkinson@chbe.ubc.ca

Bonanos[17] has proposed an alternative mechanism for hydrogen incorporation through protons in the interstitial sites of the lattice

$$1/2H_{2(g)} \Leftrightarrow H_i^{\cdot} + e' \quad [4]$$

where e' denotes a negative free electron using Kröger–Vink notation. If these reaction mechanisms were happening, an equal number of protons and electrons would be produced. As Bonanos noticed, in that case, proton conduction would always coexist with n-type electronic conduction and have a very low transport number due to the lower mobility of protons than electrons. Because this behavior is not noticed in practice, the above-mentioned mechanisms are not likely to happen. Hence, more investigation of proton creation and conduction in hydrogen containing atmospheres is required.

Proton conductivity determination.— Because $Ba_2In_2O_5$ can exhibit oxygen ion, proton, and electron conductivities under different conditions, it is important to determine the contribution of each of these conductivities to the total conductivity. One of the possible methods to distinguish the oxygen ion, electronic, and protonic conductivities in $Ba_2In_2O_5$ is to compare the total conductivity of a sample in three different atmospheres consisting of dry air, dry nitrogen, and a hydrogen containing atmosphere. In air, it is expected that $Ba_2In_2O_5$ should exhibit both oxygen ion and p-type electronic conductivity (according to Eq. 2) in addition to thermally activated n-type electronic conduction, which is expected to be negligible.[16] Hence, the measured conductivity would be given by

$$\sigma_{air} = \sigma_i + \sigma_{en} + \sigma_{ep} \quad [5]$$

where σ_{air} represents the total conductivity measured in air, σ_i is the oxygen ion conductivity, σ_{en} is the thermally activated n-type electronic conductivity, and σ_{ep} is the p-type electronic conductivity. In nitrogen, beside oxygen ion conductivity and insignificant thermally activated n-type electronic conductivity, the material can still exhibit p-type conductivity due to the presence of a very low concentration of oxygen ($P_{O_2} \sim 10^{-6}$ atm) in supplied nitrogen. However, as shown by Zhang and Smyth,[16] the p-type conductivity is very low under these conditions and can be neglected. Additional n-type electronic conductivity is expected in nitrogen under certain conditions due to the reduction of the material. The reduction is happening at oxygen partial pressures lower than 10^{-4} atm, when oxygen leaves the structure, forming oxygen vacancies and accompanying electron centers, as shown by the following reaction

$$O_O^x \Leftrightarrow 1/2O_{2(g)} + 2e' + V_O^{\cdot\cdot} \quad [6]$$

However, this process is not expected to happen below 700°C for $Ba_2In_2O_5$, as confirmed by Zhang and Smyth.[16] Consequently, the main conductivity that can be measured under nitrogen atmosphere and up to 500°C (σ_{N_2}) (as done in our tests) is the oxygen ion conductivity and the thermally activated n-type electron conductivity, given by

$$\sigma_{N_2} = \sigma_i + \sigma_{en} \quad [7]$$

If we consider σ_{en} negligible under lower temperature conditions (<700°C), the measured conductivity in nitrogen would directly determine the oxygen ion conductivity. From Eqs. 5 and 7, the p-type electronic conductivity in $Ba_2In_2O_5$ in oxidizing atmospheres can be determined from the difference of the measured conductivity in air and nitrogen

$$\sigma_{ep} = \sigma_{air} - \sigma_{N_2} \quad [8]$$

In hydrogen containing atmospheres, assuming that $Ba_2In_2O_5$ does not undergo a reduction process which would result in some electronic conduction, the measured conductivity would be the sum of the protonic conductivity, oxygen ion conductivity, and thermally activated electronic conductivity

$$\sigma_{H_2} = \sigma_{H^+} + \sigma_i + \sigma_{en} \quad [9]$$

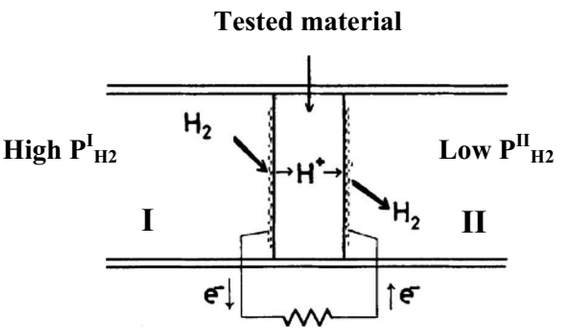

Figure 1. Schematic of emf test setup. $P^{I}_{H_2}$ is the high partial pressure of hydrogen in compartment I and $P^{II}_{H_2}$ is the low partial pressure of hydrogen in compartment II.

If the assumption is made that proton conductivity does not affect other charge carriers, the proton conductivity can be determined from the difference of the measured conductivity in hydrogen and nitrogen

$$\sigma_{H^+} = \sigma_{H_2} - \sigma_{N_2} \quad [10]$$

Another widely used method to determine the proton conductivity contribution, or proton transport number, t_{H^+} (ratio between proton conductivity and total conductivity, $t_{H^+} = \sigma_{H^+}/\sigma_t$), in oxides is the (electromotive force) emf method.[28-30] This method consists of measurement of the voltage difference across a fully dense disk sample exposed to a gradient in the partial pressure of hydrogen or water vapor, with a constant partial pressure of oxygen on both sides. The proton transport number can be determined as the ratio of the measured voltage to the theoretical electromotive force for the same conditions given by

$$E_{II-I} = -\, t_{H^+} \frac{RT}{2F} \ln \frac{P^{II}_{H_2}}{P^{I}_{H_2}} \quad [11]$$

where t_{H^+} is proton transport number, R is the universal gas constant in joules per mole kelvin, F is the Faraday constant, $P^{I}_{H_2}$ is the high partial pressure of hydrogen, and $P^{II}_{H_2}$ is the low partial pressure of hydrogen. The schematic of the emf setup is given in Fig. 1.

Beside good proton conductivity, stability of $Ba_2In_2O_5$ in hydrogen containing atmospheres is crucial if this material is to be used as a proton conductive electrolyte. Any decomposition of the material would affect its mechanical and electrical properties. Possible reduction of In^{3+} to a lower valence state could induce electronic conductivity and affect the performance of this material as a proton conductor. It is reported in the literature that $Ba_2In_2O_5$ is resistant to reduction[16,31,32] at temperatures below 700°C. Zhang and Smyth[16] showed that no n-type electronic conduction occurs in the material below 700°C due to the reduction process. Fisher et al.[31] showed that due to the high reduction energy of 4.30 eV/electron, $Ba_2In_2O_5$ is more resistant to reduction than oxidation. In their study on redox stability of $Ba_2In_2O_5$ and related compounds by cyclic voltammetry, Rolle et al.[32] confirmed a good stability of $Ba_2In_2O_5$ at 600°C up to -1 V_{ROE} in nitrogen, which corresponds to an oxygen partial pressure of 8×10^{-24} atm. A small and reversible reduction peak was observed at -1.1 V_{ROE}, which they believed was due to the reduction of In^{3+} to elemental indium. They did not observe any reduction peak that corresponds to the reduction of In^{3+} to In^{2+} or In^{1+}. In addition, they performed high-temperature X-ray diffraction (XRD) at 600°C in 1.5% H_2 for 17 h and confirmed no change in the crystal structure of $Ba_2In_2O_5$.

In this work, we report on the conductivity and stability of $Ba_2In_2O_5$ in hydrogen containing atmospheres at temperatures between 100 and 500°C. Up to date no work has been reported on the

conductivity properties of $Ba_2In_2O_5$ in hydrogen containing atmospheres, especially in the above temperature range. High proton conductivity of this and related materials in the above temperature range would create an important opportunity for use of these materials in the intermediate temperature electrochemical devices.

Experimental

$Ba_2In_2O_5$ powder samples were synthesized via the glycine–nitrate combustion process. Glycine (NH_2CH_2COOH) (Alfa Aesar, Ward Hill, MA, USA) which serves as a complexing agent and a fuel was dissolved in distilled water. Ba-acetate, [$Ba(OOCCH_3)_2$], and In-nitrate [$In(NO_3)_3 \cdot XH_2O$] (Alfa Aesar) were added in a stoichiometric ratio according to the reaction

$$2Ba(OOCCH_3)_2 + 2In(NO_3)_3 \cdot 5H_2O + 6.5O_2 \rightarrow 6NO_2 + 16H_2O + Ba_2In_2O_5 + 8CO_2 \quad [12]$$

Glycine was added in the amount to achieve a glycine/total-nitrates ratio of 5. Such a high glycine/nitrate ratio was necessary in order to prevent precipitation of Ba acetate. The solution was then heated with stirring in a glass beaker at 80°C for a few hours to complete the complexation process. The solution was transferred into a 5 l stainless steel pot and heated on a hot plate until the viscous liquid started bubbling and forming foam. The combustion happened slowly, forming a dark, very porous ash of partially reacted precursors. Additional calcining in an alumina crucible at 1300°C for 6 h was needed to achieve a pure crystalline phase. The crystal structure of the produced powder was confirmed at room temperature by powder XRD using a Bruker Corporation, East Milton, ON, Canada, AXS D8 X-ray diffractometer with a CuKα source. The thermogravimetric analysis (TGA) of the as-synthesized powders was performed using a SETARAM Inc., Newark, CA, USA, Setsys Evolution thermal analysis instrument. Tests were carried out in air with an alumina crucible up to 1500°C with a heating and cooling rate of 5°C/min.

Sample pellets for conductivity and emf measurements were prepared from produced powders by axial pressing to 150 MPa and sintering at 1400°C for 12 h. The crystal structure of the sintered samples was confirmed by X-ray diffraction. The Scherrer formula was used to calculate the grain size of produced pellets from the peak broadening in the X-ray spectra. The microstructure of the sintered samples was investigated with an Hitachi High-Technologies Canada, Inc., Toronto, ON, Canada, S-3500N scanning electron microscope (SEM). The porosity of the samples was determined by the Archimedes method. Leak tests were performed by applying a 1 psi pressure of He on the samples and measuring the leak rate with a mass flowmeter. Platinum paste was applied on both sides of the sample pellets to act as electrodes and treated to 800°C for 1 h to decompose all binders in the paste.

Electrical conductivity of the samples was determined by ac impedance spectroscopy with an impedance analyzer IM6 by ZAHNER-Elektrik GmbH & Co.KG, Kronach, Germany. Scans were done over a frequency range of 100 mHz–8 MHz, with an amplitude of 50 mV, in the temperature range of 100–500°C. The dwell time at each temperature was 3 h to allow for equilibrium to be achieved. Measurements were performed in nitrogen, air, and 50% H_2/50% N_2 atmospheres. Nitrogen and hydrogen used in the experiments (Praxair, Inc., Danbury, CT, USA) contained a maximum of 3 ppm (vol) of water and maximum 3 ppm oxygen (in N_2) and 1 ppm oxygen (in H_2). The air moisture content was about 15 ppm. Preliminary measurements were performed in all three atmospheres to determine what part of the impedance spectra was associated with the material bulk resistivity and what part with the electrode charge transfer. AC impedance tests were performed in all three atmospheres and conductivities compared to distinguish between oxygen ion, electronic, and protonic conductivities.

Proton transport numbers t_{H^+} were determined by the emf measurement using the concentration cell $P^{I}_{H_2}$, Pt‖$Ba_2In_2O_5$‖Pt, $P^{II}_{H_2}$. The sample disks were sealed to the alumina tubes on both sides of the concentration cell to avoid any leakage out of the cell. The emf of the cell was measured by a high impedance MULTISTAT 1480A-Solartron Analytical, Farnborough, Hampshire, United Kingdom. Measurements were taken at 100, 200, 300, and 400°C. The partial pressure of H_2 in both compartments was controlled by mixing H_2 with N_2 gas and water vapor at 1 atm. Water vapor concentration in the compartment I was controlled by flowing H_2/N_2 mixture through saturated vapor produced in a hot vessel at 115°C. The amount of saturated vapor in the vessel was controlled by changing the flow of the liquid water to the vessel. Water vapor concentration in the compartment II (3 vol % at all times) was set by flowing H_2/N_2 mixture through a bubbler at room temperature. The composition on the P^{II} side (low P_{H_2}) was kept constant at 48% vol H_2/49% vol N_2/3% vol H_2O. The composition on the P^{I} side was 48% vol H_2/49% vol N_2/3% vol H_2O at the beginning of each test, to determine the reference voltage when there was no gradient across the sample. This reference voltage included all unwanted voltage contributions (static charge, thermovoltage, etc.) and was deducted from the measured voltages when the gradient was present. After determining the reference voltage, the concentration on the P^{I} was changed to 80% vol H_2/15% vol N_2/5% vol H_2O, and the emf across the sample measured. The ratio of the activities of water vapor on two sides of the compartment was set to be the same as the ratio of hydrogen, so there was no gradient in oxygen activity. Measurement at each temperature was repeated three times and the standard deviation was determined. In addition to the emf tests, an electrochemical cell—air, Pt‖$Ba_2In_2O_5$‖Pt, 50% vol H_2/50% vol N_2—was constructed and the open circuit voltage (OCV) at 100, 200, 300, 400, and 500°C was measured using the MULTISTAT 1480A-Solartron.

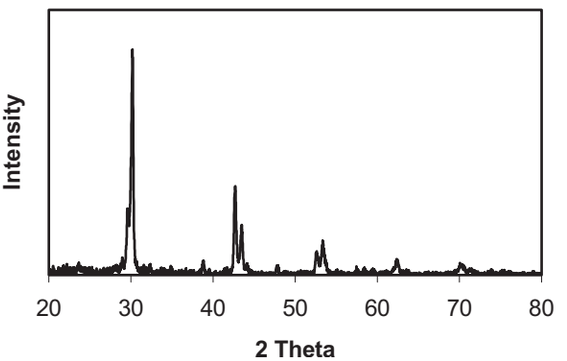

Figure 2. Typical X-ray diffraction pattern of a $Ba_2In_2O_5$ sample.

The stability of $Ba_2In_2O_5$ in a hydrogen containing atmosphere was investigated in the temperature range between 300 and 500°C. This temperature range was chosen for stability evaluation because it gave the highest conductivities. Samples were heated to temperatures of 300, 350, 400, 450, and 500°C in a 50% H_2/50% N_2 atmosphere for 24 h and ac impedance measurements were taken after 2, 8, 16, and 24 h dwell times at each temperature. X-ray diffraction measurements were performed for each sample after the testing to confirm the stability of the $Ba_2In_2O_5$ under the applied conditions. In order to confirm that there was no reduction of indium during the treatment in hydrogen, Raman analysis was performed on the samples before and after testing in hydrogen.

Results and Discussion

Crystal structure of the produced $Ba_2In_2O_5$ powder samples as well as the sintered pellets was confirmed by X-ray diffraction to be brownmillerite. Figure 2 shows XRD pattern of a typical sintered sample, confirming the brownmillerite structure. The grain size in the sintered samples was calculated to be around 40 nm using the Scherrer formula. The microstructure of a typical sintered sample is

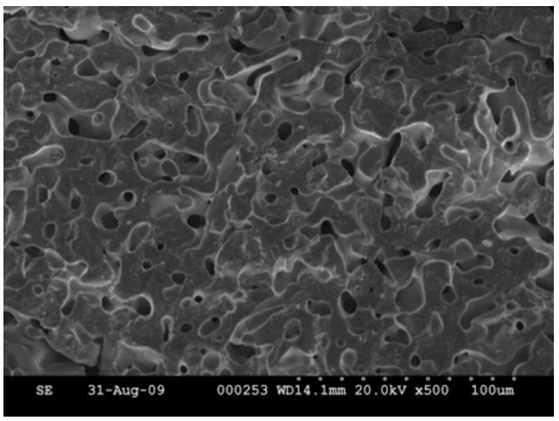

Figure 3. Typical cross-sectional SEM image of a $Ba_2In_2O_5$ sample sintered at 1400°C for 12 h.

shown in Fig. 3. Using the Archimedes method the open porosity of the samples was determined to be about 4%, while closed porosity was about 14%.

Conductivity of $Ba_2In_2O_5$.— In order to distinguish the oxygen ion, electronic, and protonic conductivities of $Ba_2In_2O_5$, conductivity measurements in three different atmospheres were performed consisting of air, nitrogen, and a hydrogen containing atmosphere in the temperature range between 100 and 500°C.

Conductivity in air.— The electrical conductivity of $Ba_2In_2O_5$ in air was measured at 100, 200, 300, 400, and 500°C. It was noticed that the conductivity of the samples depended on the treatment of the samples before the conductivity tests. Longer exposure of the sample to ambient air seemed to improve the conductivity, while heating the sample before the test seemed to reduce the conductivity. To study this behavior, two cases were investigated for each temperature tested. For case I, a fresh sample was exposed to air at 25°C for 3 days before ac conductivity measurement, and for case II a fresh sample was heated in air to 500°C for 3 h before ac conductivity testing. Figure 4 shows a characteristic ac impedance spectrum for $Ba_2In_2O_5$ measured in air for case I. The high frequency semicircle is associated with the bulk resistance, and hence, the point where this semicircle crosses the real axis is taken as the value for the bulk material resistance. A similar spectrum was obtained for case II, with a higher value for the bulk resistance.

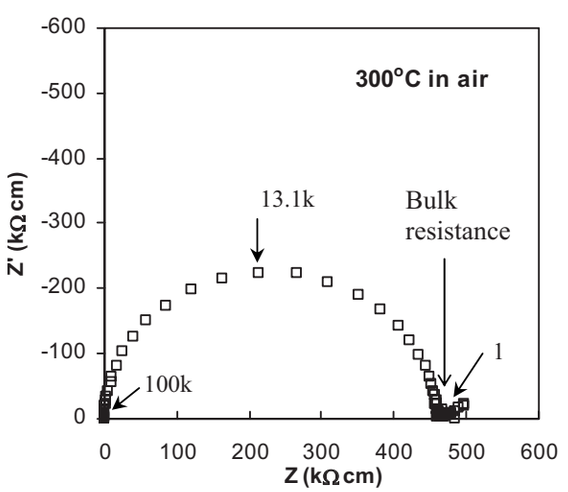

Figure 4. Typical ac impedance spectra for $Ba_2In_2O_5$ in air (case I). Frequency values (in hertz) are given for some data points on the Nyquist plot.

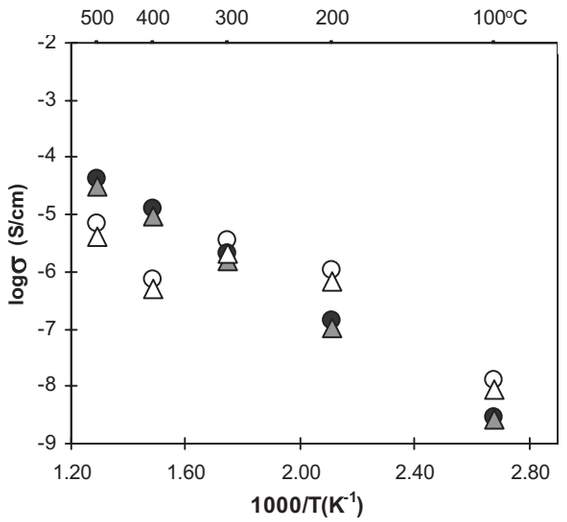

Figure 5. Arrhenius plot of $Ba_2In_2O_5$ conductivity in air and N_2: Case I (hollow symbols): fresh sample exposed to ambient air for 3 days before ac conductivity measurement in air (○) or N_2 (△); Case II (solid symbols): fresh sample treated to 500°C for 3 h before conductivity testing in air (●) or N_2 (▲).

Figure 5 shows the Arrhenius plots of $Ba_2In_2O_5$ conductivity in air for the two cases revealing different behaviors. For both the cases conductivity increases with the temperature. However, for case I, a sudden drop in conductivity occurs between 300 and 400°C, followed by a further increase in conductivity at higher temperature. This behavior for case I is likely related to the secession of H_2O bound in the $Ba_2In_2O_5$ crystal structure, which happens around 300°C. This effect has been reported by Hashimoto et al.[14] and was confirmed experimentally in our work by thermal gravimetric analysis, as shown in Fig. 6.

The process of water release starts around 260°C and is completed around 400°C. These results support the premise that water incorporated in the oxide structure at low temperatures provides protonic conductivity, which is also confirmed by Zhang and Smyth[5] by their conductivity measurements in humid air. As water leaves

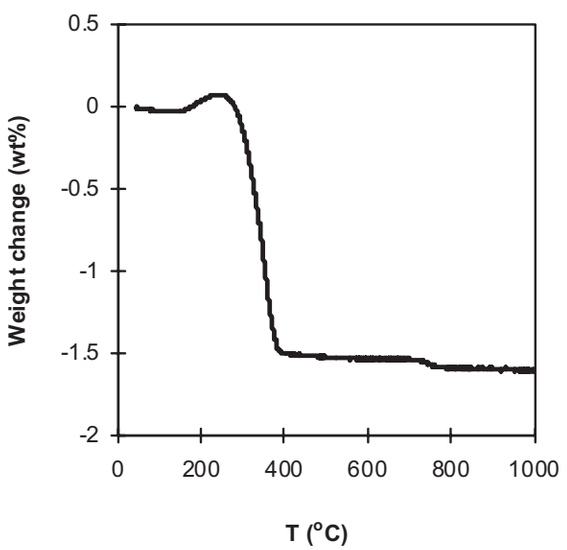

Figure 6. TGA of a $Ba_2In_2O_5$ sample in air showing a loss of water between 260 and 400°C.

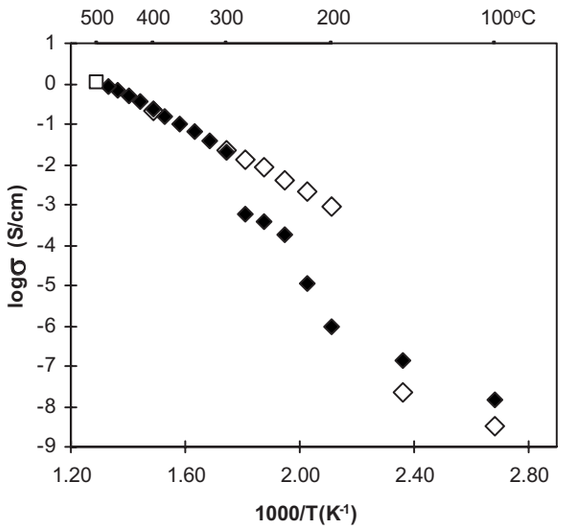

Figure 7. Arrhenius plot of $Ba_2In_2O_5$ conductivity in 50% H_2/50% N_2: Case I (♦): fresh sample exposed to air for 3 days before conductivity measurement; Case II (◇): fresh sample heated to 500°C for 3 h before testing.

the structure, the proton conductivity does not contribute anymore to the total conduction, causing it to decrease. The main charge carriers then become oxygen ions and electron holes and conductivity starts to increase again with temperature. For case II, where the sample is heated to 500°C removing all water from the structure prior to conductivity measurement, the only conductivity that was measured from the start was that from the oxygen ions and electron holes.

Conductivity in nitrogen.— For both case I and case II $Ba_2In_2O_5$ exhibited similar conductivity behavior in a nitrogen atmosphere compared to air with only slightly lower conductivity, as shown in Fig. 5. The difference in conductivity in air and nitrogen was, for example, 2.0×10^{-10} S/cm at 100°C and 9.1×10^{-6} at 500°C when measured in case II. According to Eq. 8 this difference shows the contribution of p-type electronic conduction in air, which increases with temperature, but is still very low in the temperature range from 100 to 500°C.

Conductivity in hydrogen containing atmosphere.— Again, two cases were investigated for each temperature. For case I, the fresh sample was exposed to air for 3 days to absorb water from the atmosphere before ac conductivity measurement, and for case II the fresh sample was heated to 500°C for 3 h before testing. Figure 7 shows the comparison of the measured conductivity for the two cases. Figure 8 shows typical ac impedance spectra recorded at different temperatures for case I.

At lower temperature (e.g., 100°C) a somewhat higher conductivity was measured for case I than for case II, similar to that of $Ba_2In_2O_5$ conductivity in air. This is due to the protonic conductivity provided by water bound in the material. As the temperature increased, a transitional stage was noticed for case I between 200 and 300°C, followed by surprisingly high conductivities around and above 300°C. The observed transitional stage is again due to the water release from the $Ba_2In_2O_5$ structure. In addition to TGA results this process is confirmed by a presence of a Warburg component in the ac impedance scan recorded at 260°C, as shown in Fig. 8, which reveals a diffusion process that affects the charge transfer. This temperature range again corresponds to the temperatures at which water leaves the structure, as shown in Fig. 6. With further temperature increase most of the water is released and hydrogen incorporates into the structure, significantly improving the conductivity.

For case II, most of the bound water in the sample is released to the atmosphere during the heating before testing. Lower conductivity was measured at 100 and 150°C than in case I, and the transitional range between 200 and 300°C was absent compared to that of case I. However, a sharp increase in conductivity above 150°C was noticed, most likely due to the enhanced mobility of protons above this temperature. Conductivities were significantly higher for case II versus case I in the 200–300°C range, beyond which similar conductivities were achieved. When the temperature was reduced, the measured conductivity was similar to that previously measured when increasing temperature in the range of 100–400°C, indicating no hysteresis or conductivity loss. Also, when the atmosphere was

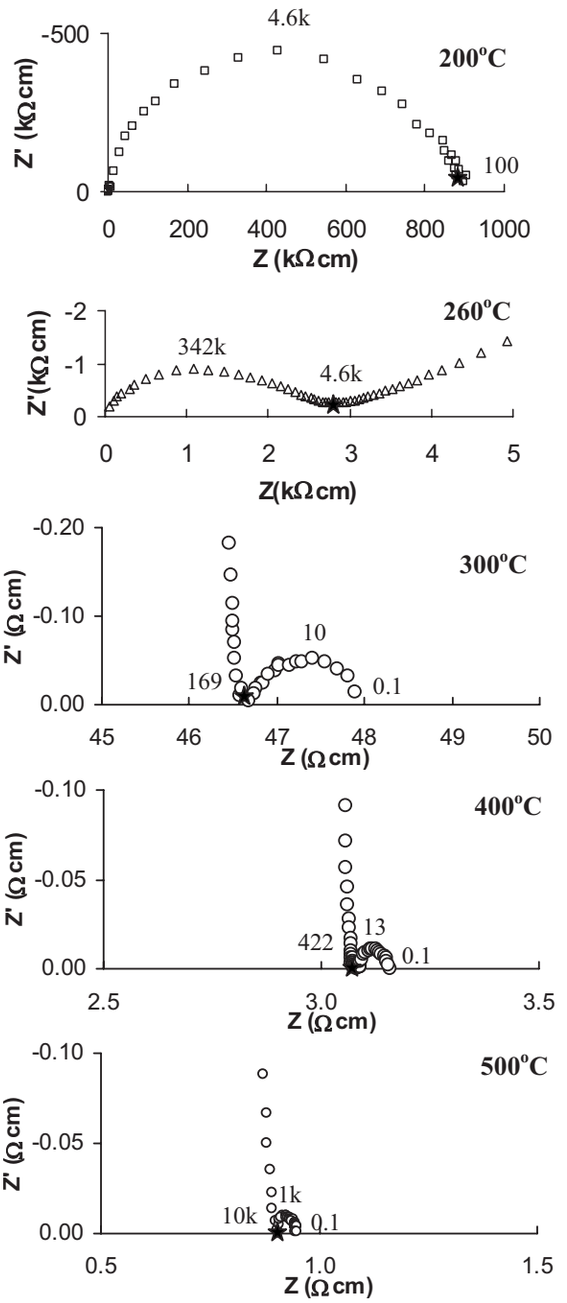

Figure 8. Typical ac impedance spectra of $Ba_2In_2O_5$ in 50% H_2/50% N_2 at different temperatures for a sample that was exposed to air for 3 days before conductivity measurement (Case I). Frequency values (in hertz) are given for some data points on the diagram. Black stars denote points taken for the bulk conductivity.

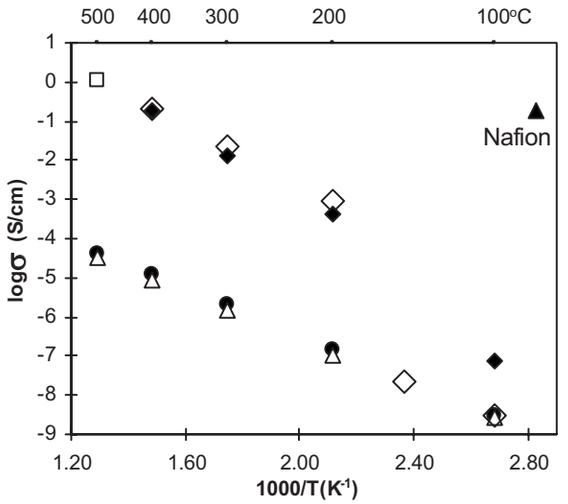

Figure 9. Comparison of $Ba_2In_2O_5$ conductivity in different atmospheres: ● in air; △ in N_2; ◇ in 50% H_2/50% N_2; ◆ in 48% H_2/49% N_2/3% steam; and □ sample decomposed. Note: In all the cases samples were heated to 500°C before testing to remove water.

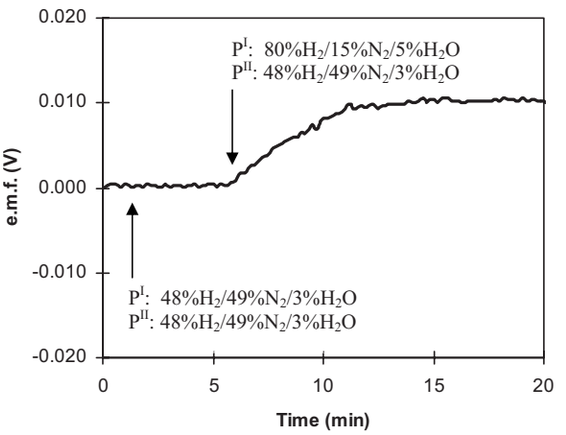

Figure 10. Measured emf across the $Ba_2In_2O_5$ sample as a function of time before and after increase in hydrogen activity in compartment I at 300°C (data corrected for unwanted voltage contributions).

switched again (e.g., from hydrogen back to nitrogen or oxygen) results were repeatable, indicating no apparent irreversible processes.

Proton conductivity of $Ba_2In_2O_5$.— In order to determine if the high conductivity of $Ba_2In_2O_5$ in hydrogen containing atmospheres is due to the proton conduction, oxygen ion, or electronic conduction, a comparison between total conductivities measured in air, nitrogen, and 50% H_2/50% N_2 was done and is shown in Fig. 9. For comparison, the conductivity of Nafion 117 submerged in water at 80°C (0.18 S/cm) was added.[33]

While at lower temperatures around 100°C, conductivities in all three atmospheres are similar, a large difference can be found at higher temperatures, with the conductivity in hydrogen atmospheres largely dominating. From these results and Eq. 10, it can be concluded that the contribution of the oxygen ion and thermally activated n-type electronic conduction is negligible in hydrogen atmospheres at temperatures above 200°C. This suggests that the dominant charge carriers are protons. The measured conductivities of 0.018–0.32 S/cm in the 300–400°C range are much higher than any reported conductivity for perovskite-related materials in hydrogen.[34] Although even higher conductivities are achieved above 400°C, the materials decompose at 500°C and above.

Proton transport numbers, t_{H^+}, for $Ba_2In_2O_5$ were determined at 100, 200, 300, 350, and 400°C by the emf method using a concentration cell $P^{I}_{H_2}$, Pt‖$Ba_2In_2O_5$‖Pt, $P^{II}_{H_2}$. When a gradient in hydrogen activity without humidification was applied across the sample, the measured emf was found to be negligible. However, when humidification was applied, much higher emfs were measured. It may be possible that a surface reduction process occurs in a highly reductive atmosphere containing hydrogen, affecting the emf measurement. With application of humidification, this process is prevented, enabling measurement of the actual emf across the sample. To make sure that humidification does not significantly affect the conductivity in a hydrogen containing atmosphere, ac conductivity was measured in a 48% H_2/49% N_2/3% H_2O atmosphere at each temperature and compared to a 50% H_2/50% N_2 atmosphere. As shown in Fig. 9, the conductivity was slightly lower in case of humidification. Emf test was then performed with the humidification. Figure 10 shows the change in voltage across the sample as the atmosphere was changed from 48% H_2/49% N_2/3% H_2O in both compartments to 80% H_2/15% N_2/5% H_2O in compartment I measured at 300°C. Table I summarizes the results of tests and the calculated proton transport numbers at different temperatures. The results reveal pure proton conductivity at lower temperatures of 100 and 200°C with high but decreasing proton transport numbers at higher temperatures. The proton transport numbers at 400°C and above could not be determined, as the sample mechanically decomposed in humid atmospheres at such high temperatures.

For additional confirmation of proton conduction, the OCV of an air, Pt‖$Ba_2In_2O_5$‖Pt, 50% H_2/50% N_2 cell was measured at different temperatures. If electronic conduction was significant, the $Ba_2In_2O_5$ would short the cell, resulting in a very low OCV. In our measurements over 3 h, we were able to obtain a constant and stable OCV of 0.8 V at 300°C, 0.64 V at 350°C, and 0.59 V at 400°C, while at lower temperatures of 100 and 200°C the values were not stable and consistent. The measured OCV values at 300, 350, and 400°C were compared to calculated values of 0.96, 0.91, and 0.87 V at these temperatures, respectively. The theoretical Nernst potential values were calculated for the temperatures of interest and partial pressures of oxygen of 0.21 atm and of hydrogen of 0.5 atm. The difference between the measured and theoretical OCV values is most likely due to a small contribution of the electronic conductivity because thick samples (~2 mm) were used to avoid leaking. However, the relatively high OCVs measured indicate that proton conductivity is predominant.

Stability of $Ba_2In_2O_5$ in hydrogen containing atmospheres.— It is important to determine the stability of $Ba_2In_2O_5$ in hydrogen containing atmospheres, especially in the temperature range where it exhibits high conductivity, i.e., 300–500°C. To determine if extended exposure to a hydrogen containing atmosphere has an effect on the conductivity and chemical stability of $Ba_2In_2O_5$, ac conductivity was measured in 50% H_2/50% N_2 at 300, 350, 400, 450, and 500°C for 24 h. X-ray diffraction measurement was performed before and after the testing. The results shown in Fig. 11 revealed that

Table I. Measured emf across the cell (80% H_2/15% N_2/5% H_2O), Pt‖$Ba_2In_2O_5$‖Pt, (48% H_2/49% N_2/3% H_2O) with standard deviation and calculated proton transport numbers (t_{H^+}) at different temperatures.

T (°C)	emf (mV)	Theoretical emf (mV) (Eq. 11)	t_{H^+}
100	8.17 ± 0.38	8.2	0.99
200	10.30 ± 0.46	10.41	0.99
300	10.56 ± 0.49	12.61	0.84
350	10.13 ± 0.32	13.71	0.74

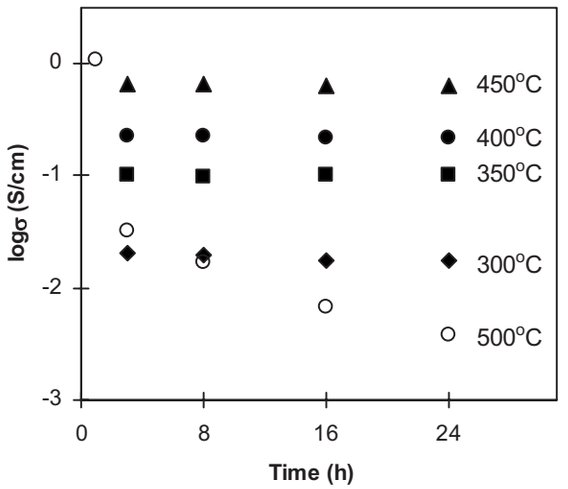

Figure 11. AC conductivity of $Ba_2In_2O_5$ in 50% H_2/50% N_2 at 300, 350, 400, 450, and 500°C for 24 h.

stable conductivities were obtained at all temperatures, except at 500°C. In addition, a 24 h test was performed at 480°C and confirmed stable conductivity. X-ray diffraction analysis before and after conductivity testing showed no change in composition at temperatures below 500°C, as shown in Fig. 12.

At 500°C, initial high conductivity decreased after first 3 h and continued to decrease with time, as shown in Fig. 11. This decrease in conductivity is due to the decomposition of the sample and contribution of the new phases to the total resistivity of the sample. The gradual appearance of the new phases is confirmed by the X-ray diffraction of the sample after 10 h and after 24 h, as shown in Fig. 13. It can be seen that $Ba_2In_2O_5$ is decomposing with time to $BaCO_3$ and elemental indium. Carbon in $BaCO_3$ is most likely originating from the incorporated CO_2 in the structure of $Ba_2In_2O_5$, as reported by Hashimoto et al.[14]

In addition to the X-ray measurements, Raman spectra were obtained for a fresh sample of $Ba_2In_2O_5$, a sample that was tested in 50% H_2/50% N_2 for 24 h at 400°C, and a sample that decomposed at 500°C, as shown in Fig. 14. A few characteristic peaks for $Ba_2In_2O_5$ (Refs. 35 and 36) were observed in the range between 100 and 610 cm^{-1}, with the most intense one at 607 cm^{-1}. In addition, a small peak at 2440 cm^{-1} is shown in Fig. 14b for $Ba_2In_2O_5$. Figure 14 shows no noticeable change between the fresh sample and the sample tested for 24 h in a hydrogen containing atmosphere. However, the Raman scan of the decomposed sample showed a change in intensity of the peaks at 485, 607, and 2440 cm^{-1}, as well as an additional peak at 2215 cm^{-1} that is associated with atomic indium and peaks at 696 and 1063 cm^{-1} associated with $BaCO_3$.[37] Thus, Raman spectra confirmed no degradation of $Ba_2In_2O_5$ at temperatures lower than 500°C, but decomposition to elemental indium and $BaCO_3$ at 500°C.

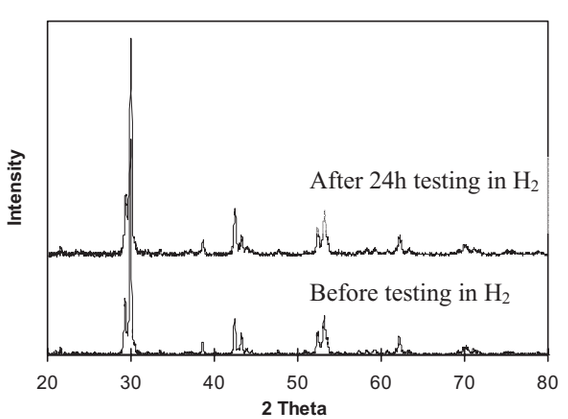

Figure 12. XRD scans of $Ba_2In_2O_5$ before and after ac conductivity testing in 50% H_2/50% N_2 at 400°C for 24 h showing no change in the structure.

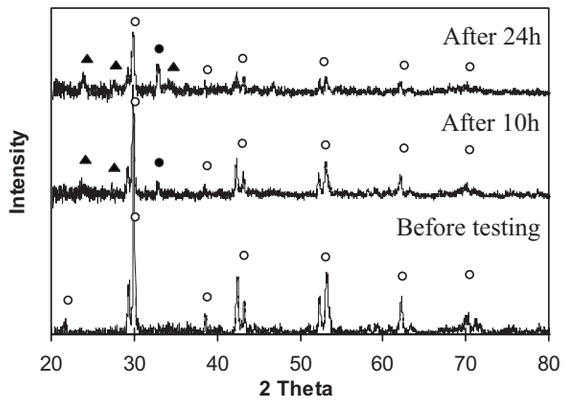

Figure 13. XRD scans of $Ba_2In_2O_5$ after ac conductivity testing in 50% H_2/50% N_2 at 500°C for 24 h: $Ba_2In_2O_5$, $BaCO_3$, elemental In.

In these studies, the testing confirmed stability of $Ba_2In_2O_5$ over 24 h in 50% H_2/50% N_2 at temperatures below 500°C and decomposition at 500°C and above. Although literature[16,31,32] reports the stability of $Ba_2In_2O_5$ in reducing atmospheres ($P_{O_2} = 10^{-19}$ atm in Ar atmosphere or 1.5% H_2 balanced by N_2), up to at least 600°C, it appears that the high concentration of hydrogen in our case is the cause for the decomposition.

Conclusions

The conductivity and stability of $Ba_2In_2O_5$ (brownmillerite phase) were tested in hydrogen containing atmospheres in the temperature range from 100 to 500°C. The conductivity was compared to the conductivity measured in air and nitrogen atmospheres. Conductivity measured in a hydrogen containing atmosphere was almost 5 orders of magnitude higher than the conductivity measured in either air or nitrogen, suggesting that the protonic conductivity in

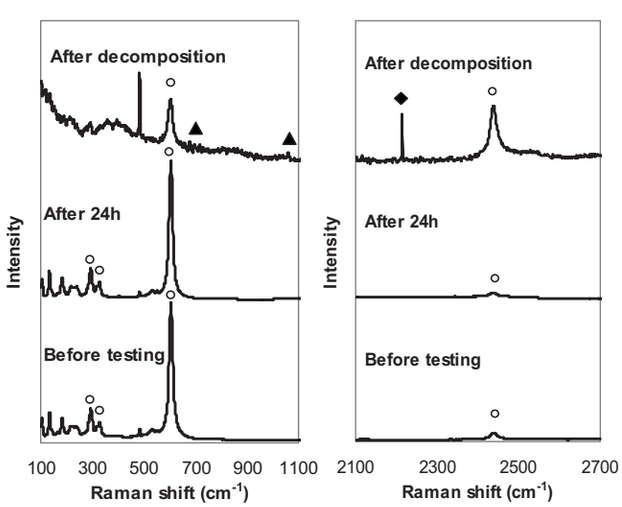

Figure 14. Raman spectra of $Ba_2In_2O_5$ before testing (bottom scan); after testing in 50% H_2/50% N_2 at 400°C for 24 h (middle scan) and after decomposition at 500°C (top scan); $Ba_2In_2O_5$, $BaCO_3$, elemental In.

$Ba_2In_2O_5$ was predominant in the hydrogen containing atmosphere. Conductivities in the range of 0.018–0.32 S/cm were measured in the 300–400°C range. The proton transport numbers determined by the emf method in a concentration cell—(80% H_2/15% N_2/5% H_2O), Pt‖$Ba_2In_2O_5$‖Pt, (48% H_2/49% N_2/3% H_2O)—were determined to be t_{H^+} = 1 at 100 and 200°C, 0.84 at 300°C, and 0.74 at 350°C. Proton transport numbers could not be determined at 400°C and above as the samples mechanically decomposed in a humidified atmosphere. However, the samples were stable up to and including 350°C. The measured OCV of the air, Pt‖$Ba_2In_2O_5$‖Pt, (50% H_2/50% N_2) cell was close to the theoretical value(s) confirming that no significant contribution from electronic conduction was present. Chemical and electrical stability of $Ba_2In_2O_5$ in hydrogen containing atmospheres was confirmed over 24 h in the temperature range from 300 to 480°C by X-ray diffraction and Raman spectroscopy as well as by consistent conductivity results over time. However, at 500°C the conductivity gradually decreased due to the decomposition of $Ba_2In_2O_5$ to $BaCO_3$ and elemental indium, which was confirmed by both X-ray diffraction and Raman spectroscopy.

The measured high electrical conductivity of $Ba_2In_2O_5$ in a reducing atmosphere in the temperature range of 300–480°C is unexpected and has not been reported before. These results are promising for the development of intermediate temperature proton-conductive materials for a range of electrochemical applications. In our future work, we plan to test the performance of this material as a proton-conducting electrolyte for an intermediate temperature fuel cell.

Acknowledgments

Financial support from the Natural Sciences and Engineering Research Council of Canada (NSERC) for this project is gratefully acknowledged. The authors thank the National Research Council Canada-Institute for Fuel Cell Innovation (NRC-IFCI) for support of this project.

University of British Columbia assisted in meeting the publication costs of this article.

References

1. T. Norby, *Solid State Ionics*, **125**, 1 (1999).
2. K. D. Kreuer, *Annu. Rev. Mater. Res.*, **33**, 333 (2003).
3. J. Niwa, T. Suehiro, K. Kishi, S. Ikeda, and M. Maeda, *J. Mater. Sci.*, **38**, 3791 (2003).
4. M. Karlsson, A. Matic, C. S. Knee, I. Ahmed, S. G. Eriksson, and L. Börjesson, *Chem. Mater.*, **20**, 3480 (2008).
5. G. B. Zhang and D. M. Smyth, *Solid State Ionics*, **82**, 153 (1995).
6. H. Iwahara, T. Esaka, and H. Uchida, *Solid State Ionics*, **3–4**, 359 (1981).
7. S. Shin, H. H. Huang, and M. Ishigame, *Solid State Ionics*, **40–41**, 910 (1990).
8. T. Yajima, H. Iwahara, and H. Uchida, *Solid State Ionics*, **47**, 117 (1991).
9. J. B. Goodenough, J. E. Ruiz-Diaz, and Y. S. Zhen, *Solid State Ionics*, **44**, 21 (1990).
10. W. Fischer, G. Reck, and T. Schober, *Solid State Ionics*, **116**, 211 (1999).
11. T. Schober, J. Friedrich, and F. Krug, *Solid State Ionics*, **99**, 9 (1997).
12. T. Schober and J. Friedrich, *Solid State Ionics*, **113–115**, 369 (1998).
13. C. A. J. Fisher and M. S. Islam, *Solid State Ionics*, **118**, 355 (1999).
14. T. Hashimoto, Y. Inagak, A. Kishi, and M. Dokiya, *Solid State Ionics*, **128**, 227 (2000).
15. P. Berastegui, S. Hull, F. J. Garcia-Garcia, and S.-G. Eriksson, *J. Solid State Chem.*, **164**, 119 (2002).
16. G. B. Zhang and D. M. Smyth, *Solid State Ionics*, **82**, 161 (1995).
17. N. Bonanos, *Solid State Ionics*, **53–56**, 967 (1992).
18. R. Hui, R. Maric, C. Decès-Petit, E. Styles, W. Qu, X. Zhang, J. Roller, S. Yick, D. Ghosh, K. Sakata, et al., *J. Power Sources*, **161**, 40 (2006).
19. R. J. D. Tilley, *Principles and Applications of Chemical Defects*, p. 103, Stanley Thornes Publishers Ltd., Cheltenham, United Kingdom (1998).
20. H. Iwahara, H. Uchida, K. Ono, and K. J. Ogaki, *J. Electrochem. Soc.*, **135**, 529 (1988).
21. H. Iwahara, T. Yajima, T. Hibino, K. Ozaki, and H. Suzuki, *Solid State Ionics*, **61**, 65 (1993).
22. W. K. Lee, A. S. Nowick, and L. A. Boatner, *Solid State Ionics*, **18–19**, 989 (1986).
23. T. Scherban, A. S. Nowick, L. A. Boatner, and M. M. Abraham, *Appl. Phys. A*, **55**, 324 (1992).
24. T. Shimura, M. Komori, and H. Iwahara, *Solid State Ionics*, **86–88**, 685 (1996).
25. T. Shimura, K. Suzuki, and H. Iwahara, *Solid State Ionics*, **113–115**, 355 (1998).
26. P. Murugaraj, K. D. Kreuer, T. He, T. Schober, and J. Maier, *Solid State Ionics*, **98**, 1–2 (1997).
27. G. Ma, F. Zhang, J. Zhu, and G. Meng, *Chem. Mater.*, **18**, 6006 (2006).
28. T. Norby, *Solid State Ionics*, **28–30**, 1586 (1988).
29. D. P. Sutija, T. Norby, and P. Bjiirnbom, *Solid State Ionics*, **77**, 167 (1995).
30. H. H. Uchida, N. Maeda, and H. Iwahara, *J. Appl. Electrochem.*, **12**, 645 (1982).
31. C. A. J. Fisher, M. S. Islam, and R. J. Brook, *J. Solid State Chem.*, **128**, 137 (1997).
32. A. Rolle, G. Fafilek, and R. N. Vannie, *Solid State Ionics*, **179**, 113 (2008).
33. N. Sammes, *Fuel Cell Technology-Reaching Toward Commercialization*, Springer, New York (2006).
34. H. J. Park, C. Kwak, K. H. Lee, S. M. Lee, and E. S. Lee, *J. Eur. Ceram. Soc.*, **29**, 2429 (2009).
35. J. F. Q. Rey, F. F. Ferreira, and E. N. S. Muccillo, *Solid State Ionics*, **179**, 1029 (2008).
36. A. Rolle, S. Daviero-Minaud, P. Roussel, A. Rubbens, and R. N. Vannier, *Solid State Ionics*, **179**, 771 (2008).
37. P. Chinho, J. Woo-Sik, Z. Huang, and A. Timothy, *J. Mater. Chem.*, **12**, 356 (2002).